Available online at www.sciencedirect.com
ScienceDirect
Polymer 48 (2007) 3494–3503
polymer
www.elsevier.com/locate/polymer

The use of THz time-domain reflection measurements to investigate solvent diffusion in polymers

Jelena Obradovic [a], James H.P. Collins [b], Ole Hirsch [a], Michael D. Mantle [b], Michael L. Johns [b,*], Lynn F. Gladden [b]

[a] *Department of Physics, Cavendish Laboratory, University of Cambridge, J.J. Thomson Avenue, Cambridge CB3 0HE, United Kingdom*
[b] *Department of Chemical Engineering, University of Cambridge, Pembroke Street, Cambridge CB2 3RA, United Kingdom*

Received 13 February 2007; received in revised form 10 April 2007; accepted 11 April 2007
Available online 19 April 2007

Abstract

Solvent diffusion into polymers is central to their performance, for example as controlled delivery pharmaceutical products. In this work, we present the novel application of terahertz (THz) time-domain reflectance spectroscopy to quantify the ingress of acetone into various polymer materials. Reflections from the top and bottom surfaces of the discs are temporally resolved, as is a reflection from the interface between acetone-wet polymer and dry polymer. These reflections enable both the polymer swelling and more importantly the position of the liquid diffusion front to be quantified as a function of time. Verification of these measurements is provided by equivalent magnetic resonance imaging (MRI) measurements, with which there is excellent agreement.

Keywords: Terahertz reflection spectroscopy; Diffusion; MRI

1. Introduction

In the past few decades, the ingress of liquid solvent molecules into solid polymers has attracted much attention, both with respect to their manufacture and ultimate use. In certain applications (e.g. pharmaceutical devices [1]) this solvent transport is desirable, however, in others it causes degradation and contamination of the polymer (e.g. packaging [2]). Accurate measurement of the liquid ingress position is desirable for the validation of models of this process, improved understanding of the liquid penetration process and potentially the provision of on-line or by-line measurement during processing or storage. In the current paper we report on the novel application of THz time-domain reflection spectroscopy to measure the penetrant front position in various polymers.

Analysis of liquid uptake by solid polymeric systems, and subsequent structural changes within the polymer, can be conducted with a range of techniques. These include destructive techniques, such as gravimetric [3,4] and thermogravimetric [5] methods, as well as sectioning the polymer in order to enable access for optical microscopy [3,6]. Infrared-attenuated total reflection spectroscopy [7] and Rutherford backscattering spectrometry [8] enable the amount of liquid or gas penetrant in very thin polymer sheets to be measured as a function of time, in addition to potentially providing some spectroscopic information about the molecular state of the penetrant liquid molecules. Non-destructive alternatives for relatively thick polymer samples include X-ray microtomography [9], in which *in situ* measurement of penetrant depth is complicated by the necessity of operating a closed system, and Magnetic resonance imaging (MRI). MRI techniques have found extensive application in the literature with respect to imaging liquid ingress into polymer systems [2,10,11].

In the current paper we report the novel application of THz time-domain reflection spectroscopy to measure the penetrant

* Corresponding author. Tel.: +44 (0) 1223 334767; fax: +44 (0) 1223 334796.
E-mail address: mlj21@cam.ac.uk (M.L. Johns).

0032-3861/$ - see front matter © 2007 Elsevier Ltd. All rights reserved.
doi:10.1016/j.polymer.2007.04.010

Nomenclature

a	shift of the reflection point
c	speed of light
d	thickness of the dry polymer
d_a	thickness of the unpenetrated polymer layer
d_b	thickness of the acetone-wet polymer
$d_{b(corrected)}$	thickness of the acetone-wet polymer corrected for the amount of swelling
H	hydrogen atom
K	constant
Δl	amount of swelling
m	constant
n_1	refractive index of air
n_2	refractive index of dry polymer
n_3	refractive index of acetone-wet polymer
t	time
Δt	time delay at the detector
t_1	arrival time at the detector of the reflection from the top polymer surface
t_2	arrival time at the detector of the reflection from the dry polymer–acetone-wet polymer interface
t_3	arrival time at the detector of the reflection from the bottom polymer surface
Δx	difference in path lengths
x_1	path length difference in air
x_2	path length difference in polymer
α	angle of incidence from air
β	angle at which the THz beam is refracted when propagating from air to the polymer disc
γ	angle at which the THz beam is refracted when propagating from dry polymer to the acetone-wet polymer.

front position of acetone in various polymers (polycarbonate and PVC) *in situ*, and thus as a function of time and temperature. Our data are verified by detailed comparison with MRI measurements on the same systems. Application of THz spectroscopy and imaging increased rapidly over recent years, largely due to advances in ultra-fast laser technology and the consequential development of compact THz sources and detectors [12–14]. Applications include characterisation of materials [15], in the fields of medicine [16,17], and pharmaceuticals [18]. The potential of THz time-domain reflection spectroscopy has been demonstrated for the analysis of tablet coating thickness in pharmaceutical systems [19] and for the study of human skin [20]. In our work, the reflection of a short THz pulse off a penetrant front is observed. Such a measurement is readily applied to any polymer geometry (e.g. polymer sheets), and is consequently arguably more suited to on-line and by-line measurement than MRI techniques.

2. Background

Transport of solvent molecules into polymeric systems depends on both the diffusive properties of the solvent molecule and any resultant conformational changes in the polymer. Three broad classifications describe solvent transport in polymers, generally referred to as Case 1, Case 2 and anomalous diffusion. Such classification depends on the rate of solvent diffusion into the polymer relative to the rate of relaxation and reorganisation of the polymer [21], and hence on which controls the ingress process. In Case 1 diffusion, the diffusion rate controls the liquid ingress; in Case 2 diffusion, polymer chain relaxation is rate-controlling and anomalous diffusion occurs when the rates are of similar magnitude. The relative contribution of solvent diffusion and polymer relaxation can often be determined based on the following phenomenological relationship between the depth of penetration, d_b and time, t [22]:

$$d_b(t) = Kt^m, \tag{1}$$

where K and m are constants. Case 1 transport is characterised by $m = 1/2$, Case 2 by $m = 1$ and for 'anomalous' diffusion m can take any intermediate value between 1/2 and 1. Since the position of the liquid penetration front is generally correlated with the mass uptake at various times, the form of Eq. (1) can also be used to describe such mass uptake data.

The polymer relaxation times are associated with structural changes in the polymer system and will consequently vary with temperature. The diffusion coefficient of the penetrate will also increase with temperature. Thus it is possible that classification of a particular penetrant and polymer system as Class 1, Class 2 or anomalous diffusion may vary with temperature [23].

3. Experimental

3.1. Samples used and their preparation

Acetone (Fisher Scientific, Analytical Grade 99.5%) was used as a model penetrant. Two polymeric systems were considered – polycarbonate (Licharz Ltd., density 1.20 g/cm^3) and polyvinylchloride (PVC, Licharz Ltd., density 1.42 g/cm^3). Both were cut from sheets into 20 mm diameter discs, the polycarbonate was 1.93 mm thick and the PVC was initially 3 mm thick, but was filed down to a thickness of 2 mm.

For THz measurements, only the rear surface of the polymer discs was exposed to acetone by placing the discs on a perforated PTFE support ring of outer diameter 19.0 mm; a photograph of the support ring is shown in Fig. 1. The disc was then placed in a PTFE cavity of inner diameter 23.5 mm (also shown in Fig. 1), which was continuously topped up with acetone to ensure a consistent contact between the acetone and the rear surface of the polymer disc. This arrangement allowed a THz pulse to be applied to the polymer disc sample from above.

For MRI measurements, a PTFE sample tube holder was made with an inner diameter of 23.0 mm, into which the discs were placed. The discs were only exposed to acetone from below in order to mimic acetone ingress during the THz measurements. The discs were then removed from the acetone

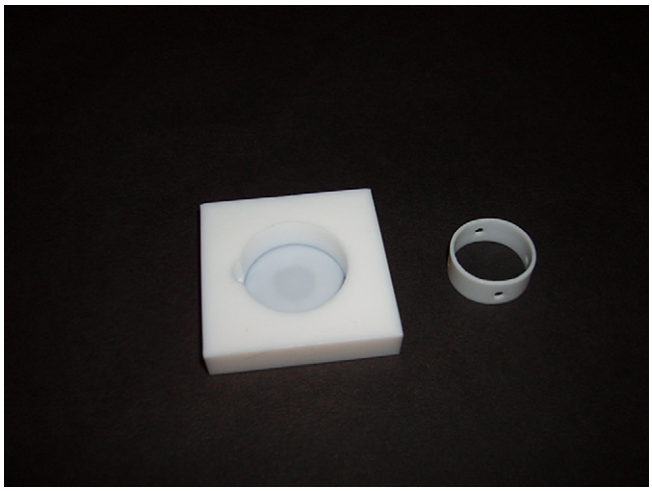

Fig. 1. PTFE cavity for containment of the acetone – shown on the left hand side of the picture, and perforated PTFE ring used as a support of the polymer disc – shown on the right hand side of the picture.

after a specified period of time and a thin layer of silicon sealant gel was applied to the unexposed top surface (this acted as a geometric reference point for the subsequently acquired images) and then placed in the MRI spectrometer magnet. Images of the discs were acquired immediately. Although it is possible to image liquid ingress into polymers *in situ* with MRI, our measurements were performed *ex situ* in order to better mimic the THz measurements, in particular maintenance of the height of the acetone pool which is not visible within the magnet.

3.2. Terahertz time-domain reflection spectroscopy

The THz experiments were performed using a time-domain spectroscopy system in reflection geometry, which is shown schematically in Fig. 2. A Ti:sapphire laser (Femtosource compact, Femto Lasers, Austria) provides a train of laser pulses of 10 fs duration, with a repetition rate of 75 MHz, centred at a wavelength of 790 nm. These optical pulses are split into a pump beam for THz generation and a probe beam for detection. The pump beam is used for generation of THz pulses by photo-excitation of a gallium arsenide (GaAs) photoconductive antenna typically biased between 70 and 100 V. A laser pulse, focused onto the gap between two gold electrodes deposited onto GaAs wafer, creates electron-hole pairs in the semiconductor. These electron-hole pairs then accelerate in the electric field created by the bias applied to the electrodes. The accelerated carriers give rise to photo-current, which decays according to a time constant determined by the lifetime of the carriers of the semiconductor. Electromagnetic waves in the THz frequency range are emitted during this process. Emission from the photoconductive antenna is strongly influenced by the antenna design [24,25].

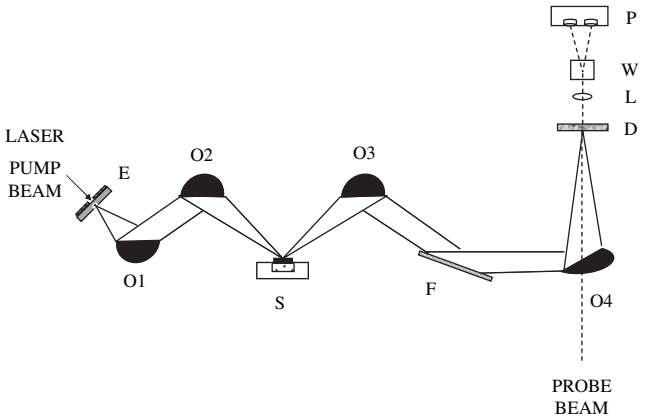

Fig. 2. Schematic diagram of the reflectance spectrometer. E: emitter; O: off-axis parabolic mirrors; F: flat mirror; S: sample holder with polymer disc; D: detector; L: lens; W: Wollaston prism; P: photodiodes.

With reference to Fig. 2, the THz beam emitted from the GaAs antenna passes through a series of off-axis parabolic mirrors and is focused on the unexposed top surface of the polymeric disc. The beam is incident upon the sample at an angle of 50° to normal incidence. The THz beam size on the sample is approximately 2 mm in diameter and is positioned in the centre of the disc surface. The reflected THz pulses are then recollimated using another pair of off-axis parabolic mirrors and focused onto a 2 mm thick zinc telluride (ZnTe) detector. Electro-optic sampling was used for detection of THz waves. The THz field modulates the birefringence of a ZnTe crystal (Pockel's effect [26]). The linear polarisation of the laser probe beam is changed accordingly, while passing through the detector crystal. A quarter wave plate behind that crystal measures this change by producing either circularly or elliptically polarised radiation from the incoming probe beam. The two orthogonally polarised components of the probe beam are then separated by a Wollaston prism. In this way the differences in the intensity of those two components are the measure of the THz electric field strength. A pair of balanced photodiodes registers the difference. This electric difference signal is the input to a lock-in amplifier. Reference for the lock-in is provided by electric modulation of the pump beam at 20 kHz. By systematically varying the delay between pump beam and probe beam, the time of the THz pulse was measured.

When the THz pulse was applied to the top surface of the polymeric disc, part of the incident THz pulse was reflected from the surface. The rest passed into the sample and was partially reflected every time it encounters a new dielectric interface characterised by a different index of refraction. A typical time-domain THz signal is shown in Fig. 3. During solvent penetration, three usually distinct THz reflection signals were observed at the detector at times, t_1, t_2, and t_3 (as indicated in Fig. 3):

- The reflection at t_1 results from the top surface of the polymer (and hence arrives first at the detector) – this moves to shorter times as the polymer swells in response to acetone ingress.
- The reflection at t_2 originates from the interface between 'dry' and 'acetone-wet' polymer. This corresponds to the position of the diffusion front and moves to shorter times as the acetone penetrates further inwards from the rear surface of the polymer disc.

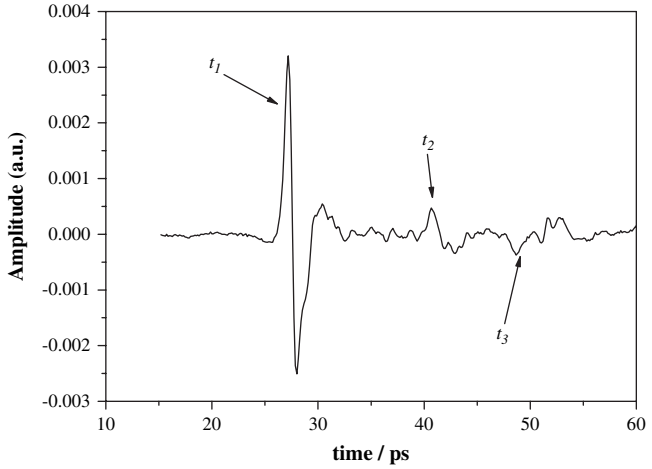

Fig. 3. A typical time-domain THz signal obtained in reflection geometry with reflection peaks originating from different interfaces at the following times: t_1: reflection from the top surface of the polymer disc; t_2: reflection from the advancing liquid front within the polymer; t_3: reflection from the rear side of the polymer disc.

- The reflection at t_3 originates from the rear surface of the polymer disc. This reflection gradually diminishes in magnitude with exposure time; as more acetone is absorbed by the polymer, the THz beam reaching this interface is increasingly attenuated.

For the PVC samples, 20 averages were used to produce each time-domain signal, resulting in a minimum acquisition time of 6.5 min. For the polycarbonate, 10 averages were used to produce each time-domain signal, resulting in a minimum acquisition time of 5 min. THz reflection measurements were acquired periodically during acetone ingress for each experiment. In order to investigate the ingress process as a function of temperature, the PTFE sample holder was replaced with a stainless steel one (improved thermal conductivity) of inner diameter 21.86 mm and placed on a 70 W Peltier element with temperature control (±1 °C). This was only performed with the PVC for which literature values are available for comparison, at temperatures of 13, 25 and 40 °C [4]. Measurement ceased when the polymer discs become visibly bent due to acetone ingress. This occurred at shorter times for higher temperatures, as would be expected. This was the limiting factor in the total time over which ingress could be observed, as the accuracy of the THz pulse path length is compromised.

3.3. THz data analysis method

The polymer disc cross-section and the formation of different THz reflections are schematically presented in Fig. 4. The arrivals of different reflections at the detector are delayed due to the additional path length that is propagated by the portion of the THz beam refracted at the various interfaces. The length difference, Δx, between the paths travelled by the subsequent reflections from the air-dry polymer and dry polymer–wet polymer, arriving at the detector, is given by (derivation presented in Appendix A):

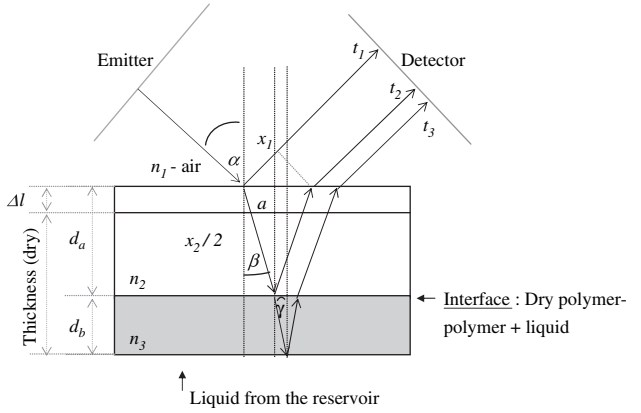

Fig. 4. Schematic cross-section of THz reflections from the polymer disc. n_1: index of refraction of air; n_2: index of refraction of dry polymer; n_3: index of refraction of the polymer penetrated by the liquid; α: angle of incidence from air; β: angle at which the THz beam is refracted when propagating from air into the polymer disc; a: shift of the reflection point; x_1: path length difference in air; x_2: path length difference in dry polymer; d_a: thickness of the unpenetrated polymer layer; d_b: thickness of the acetone-wet polymer layer; Δl: amount of swelling.

$$\Delta x = x_2 - x_1 = \frac{2d_a}{\cos\beta}(1 - \sin\beta\sin\alpha), \tag{2}$$

where d_a is the thickness of the unpenetrated polymer layer, α represents the angle of incidence from air (50°) and β is the angle at which the THz beam is refracted when propagating from air to the polymer disc and is determined using Snell's law [25]:

$$\frac{\sin\alpha}{\sin\beta} = \frac{n_2}{n_1}. \tag{3}$$

The value of n_1, the refractive index of air, is 1. The value of n_2, the refractive index of the polymer disc, is determined using the THz spectroscopy system in transmission geometry as described in Ref. [27]. The THz pulses were recorded with and without the polymeric disc placed at a focal plane of the beam. Measuring the time delay caused by the additional optical path length introduced by the polymeric disc with known thickness, the indices of refraction, n_2, are determined as 1.62 for polycarbonate and 1.63 for PVC.

The time delay at the detector introduced by this difference in path lengths, Δx, is:

$$\Delta t = t_2 - t_1 = \frac{x_2 n_2}{c} - \frac{x_1 n_1}{c} = \frac{2d_a(t)}{c\cos\beta}(n_2 - n_1\sin\beta\sin\alpha). \tag{4}$$

The arrival times t_1 and t_2 are obtained from the positions of the reflection peaks as shown in Fig. 3, and correspond to the maximum positive THz signal intensity. Hence application of Eq. (4) allows the value of $d_a(t)$ to be calculated. Consequently we can calculate the thickness of the acetone-wet polymer layer, d_b, as a function of time:

$$d_b(t) = d + \Delta l(t) - d_a(t), \tag{5}$$

where d denotes the thickness of the completely dry polymer and $\Delta l(t)$ is the increase in thickness of the polymer disc due to swelling. $\Delta l(t)$ can be calculated as a function of time:

$$\Delta l(t) = \frac{c(t_1(0) - t_1)}{2\cos\alpha}, \quad (6)$$

where $t_1(0)$ is the reflection time from the top surface of the polymer disc before the introduction of acetone. Since the base or rear of the polymeric disc was supported by the PTFE ring, net increase in overall thickness of the disc due to swelling only occurred in an upward direction. The acetone front position, d_b, can be recalculated, accounting for the swelling that has occurred. This 'corrected' front $d_{b(corrected)}$ corresponds to the hypothetical position of the front if the polymer did not swell:

$$d_{b(corrected)}(t) = d_b(t) - \Delta l(t). \quad (7)$$

3.4. Magnetic resonance imaging

All MRI experiments were conducted using a Bruker Biospin AV 400 NMR spectrometer, corresponding to a ^{1}H resonance frequency of 400.23 MHz. A ^{1}H birdcage radio-frequency (RF) coil, with an internal diameter of 25 mm, was used to both excite and detect the spin system under study. A 2D image was acquired in a vertically orientated slice of thickness 2 mm using a standard spin-echo imaging pulse sequence [28]. The echo time was adjusted to 5 ms in order to reduce T_2 relaxation effects. The recycle time used was sufficiently large so as to eliminate any T_1 relaxation contrast. The slice was positioned perpendicular to the exposed rear surface through the centre of the disc. This image consisted of 128 (in the vertical direction) $\times$ 16 (in the radial direction) voxels with a field of view of 5 mm $\times$ 25 mm corresponding to an anisotropic voxel size of 0.039 $\times$ 1.563 mm^2. The central vertical slice of the resulting 2D image was then extracted from the 2D data set and used to generate a 1D vertical profile of acetone penetration into the disc. This allowed acetone penetration into the edges of the disc to be ignored, in addition to measuring the acetone front position and swelling at the same location as in the THz experiments. The experiments were repeated using a new polymer disc for each immersion time investigated.

Similar experiments conducted using deuterated acetone (Sigma–Aldrich), show that the ^{1}H signal in the polycarbonate discs is only due to the infiltrating acetone and not due to polycarbonate. Thus the ^{1}H signal obtained is directly proportional to the concentration of acetone. However, in the PVC disc samples approximately 50% of the ^{1}H signal intensity is due to mobilised polymer. This does not compromise accurate determination of the start of the penetrant front but could distort the front shape and calculations of quantitative acetone concentration profiles.

3.5. MRI data analysis

The 1D profiles were analysed to determine the position of the acetone front, $d_b(t)$, and the total thickness of the sample, $d + \Delta l(t)$. The upper surface of the polymer is distinct due to the signal received from the sealant gel and can thus be used as a geometric reference point. The rear surface of the disc is taken as the point when the signal from the acetone becomes less than the inherent background noise. The position of the front was initially assumed to be the position of maximum gradient in measured signal intensity. In the case of the polycarbonate, the penetrant front was quite distinct and narrow. For the PVC, a comparatively broad penetrant front is evident, consequently the position of maximum acetone signal intensity and the leading edge of the front were also measured (defined as the position along the front where the signal intensity becomes less than the inherent noise level).

4. Results and discussion

4.1. THz results

Fig. 5(a) shows THz time-domain measurements presented as a stack plot against acetone exposure time. The reflections from the top surface at time t_1, the penetrant front interface at

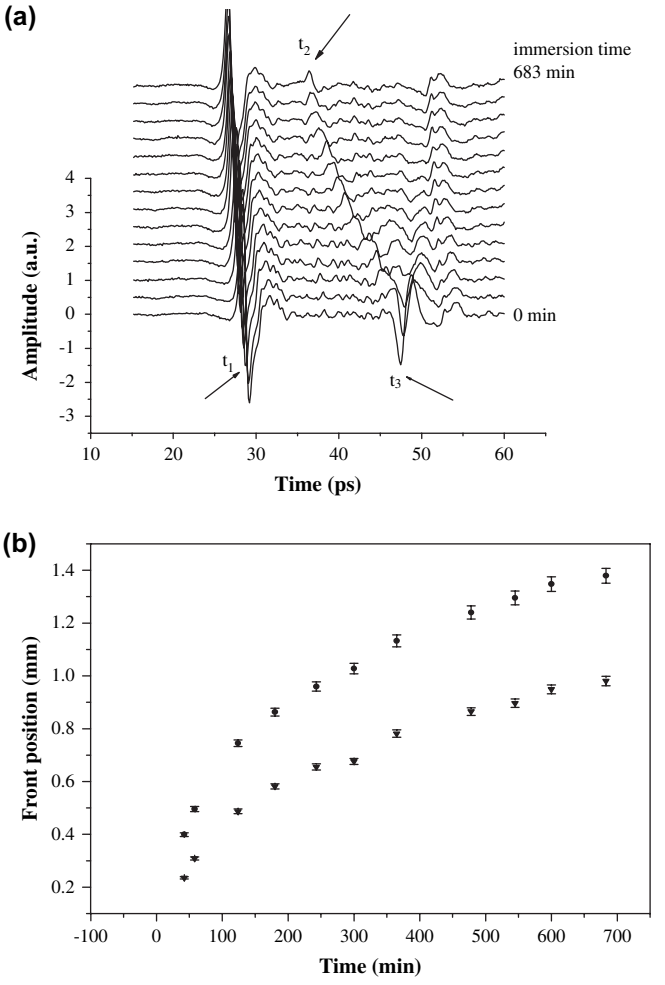

Fig. 5. (a) THz time-resolved measurement of acetone diffusion into polycarbonate at room temperature. The waveforms were recorded (starting from dry, 0 min) at: 5, 23, 42, 58, 124, 180, 243, 300, 365, 473, 545, 600 and 683 min. (b) The acetone front positions d_b (●) and $d_{b(corrected)}$ (▼) are shown as a function of acetone exposure time. The error bars are determined from the width at half maximum of the reflected pulses.

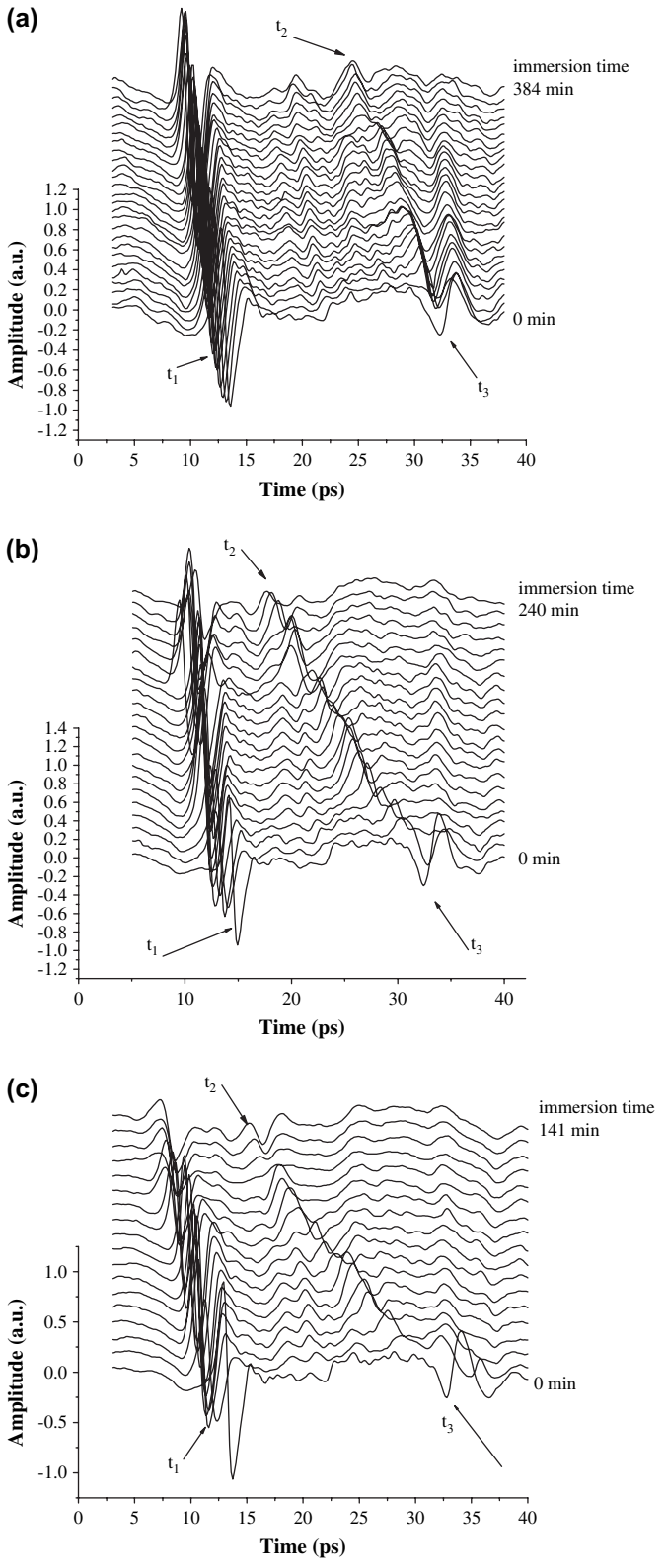

Fig. 6. Time evolution of the acetone penetration front in PVC discs at (a) 13 °C, (b) 25 °C and (c) 40 °C. Measurements were taken (starting from dry polymer) at the following times: 1, 9, 17, 24, 31, 38, 47, 54, 64, 73, 82, 94, 101, 111, 120, 133, 150, 180, 212, 248, 276, 300, 316, 330, 356 and 384 min for 13 °C; 1, 7, 15, 23, 32, 39, 46, 53, 64, 73, 82, 94, 101, 111, 119, 130, 141, 150, 180, 211 and 240 min for 25 °C and at: 1, 9, 17, 23, 31, 38, 46, 53, 64, 73, 82, 94, 101, 111, 119, 130 and 141 min for 40 °C.

time t_2 and the rear surface of the polymer at time t_3 are all evident. At comparatively short times (<42 min), it is difficult to resolve the reflections at times t_2 and t_3. As penetration of acetone proceeds, the reflection at time t_2 shifts towards the top surface of the polymer. The resultant calculated positions of the penetration front, d_b and $d_{b(corrected)}$, are shown in Fig. 5(b), as a function of acetone exposure time. The difference reflects the extent of polymer swelling. The error bars are determined by the temporal width of the reflections at half maximum.

Fig. 6(a–c) shows stacked THz time-domain measurements of the acetone ingress into PVC discs at 13, 25 and 40 °C, respectively. Fig. 7(a) and (b) shows the calculated values of d_b and $d_{b(corrected)}$, as a function of acetone exposure time. As the temperature was elevated from 13 to 40 °C, the acetone

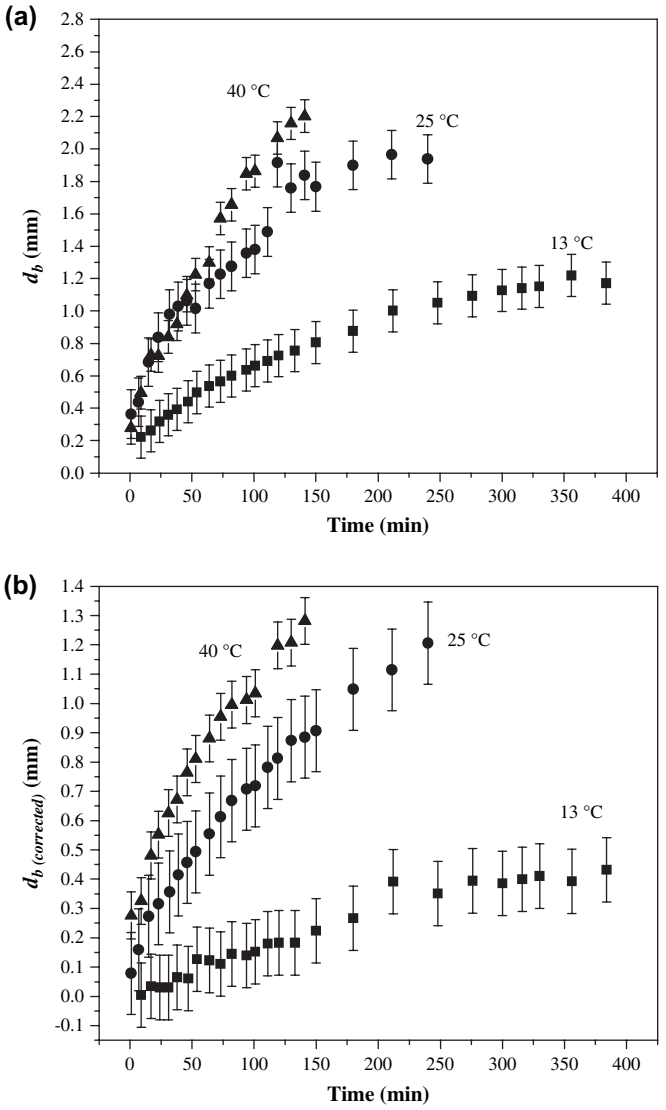

Fig. 7. Comparison of the penetration front of acetone into PVC discs at 13 °C (■), 25 °C (●), 40 °C (▲): (a) the calculated front position d_b; (b) the recalculated value $d_{b(corrected)}$ obtained when polymer swelling was accounted for. The error bars are determined from the width at half maximum of the reflected pulses.

penetration front moved towards the top surface much faster, as would be expected due to the increased temperature increasing both the acetone diffusion and the polymer motion. Evident in Fig. 6, and to a less extent in Fig. 5, are 'noise' oscillations, smaller than the main reflections at times t_1, t_2 and t_3. These arise from a number of effects, mainly from absorption of THz radiation by water vapour in the THz beam path. They do not, however, severely compromise determination of the position of the three reflections of interest.

4.2. Comparison with MRI

Sample MRI 1D profiles for acetone ingress into polycarbonate are shown in Fig. 8(a) at acetone exposure times of 42, 300 and 545 min. Peak 1 corresponds to the sealant and was used as a geometric reference to align the profiles recorded from different samples. The penetrant front corresponds to position 2 and clearly moves towards the top surface of the polymer with exposure time. Position 3 is the rear side of the polymer. The unusual shape of the penetrant front will be discussed below. Fig. 8(b) shows sample profiles for acetone ingress into the PVC sample at 25 °C. The broader front, relative to the polycarbonate, is clearly evident.

In Fig. 9 the acetone front position, $d_{b(corrected)}$, as determined by analysis of the MRI data, is presented along with the corresponding THz data for ingress into the polycarbonate sample. Error bars for the THz data are determined by the width of the reflected pulse at half maximum (as in Figs. 5(b) and 7); error bars for the MRI data result from the discrete nature of the MRI data (±1 voxel). The polycarbonate results show good agreement between the MRI and THz experiments. Fig. 10 presents the corresponding comparison of MRI and THz data for the PVC system for (a) 25 °C and (b) 40 °C, respectively. Agreement between the two measurement methods is reasonably good. The existence of a distinct reflection between wet and dry polymers for the PVC system (as seen in Fig. 6) is not intuitive, given the broad ingress front revealed by MRI (Fig. 8(b)). For the MRI data we have defined the front position as the point of maximum gradient. To better ascertain what part of the ingress front is resulting in the THz reflection, we also determined from the MRI data, the start point of the front (defined as the position along the front when the MRI signal level falls below the noise level), our existing definition of maximum gradient in signal intensity and the front end (defined as the point of maximum signal intensity in the MRI profile data). These data (d_b) are plotted in Fig. 11 for both (a) 40 °C and (b) 25 °C, respectively. For the sake of presentation clarity, the data are plotted without error bars. What is evident in Fig. 11 is that the position of maximum gradient and the start of the front are in very

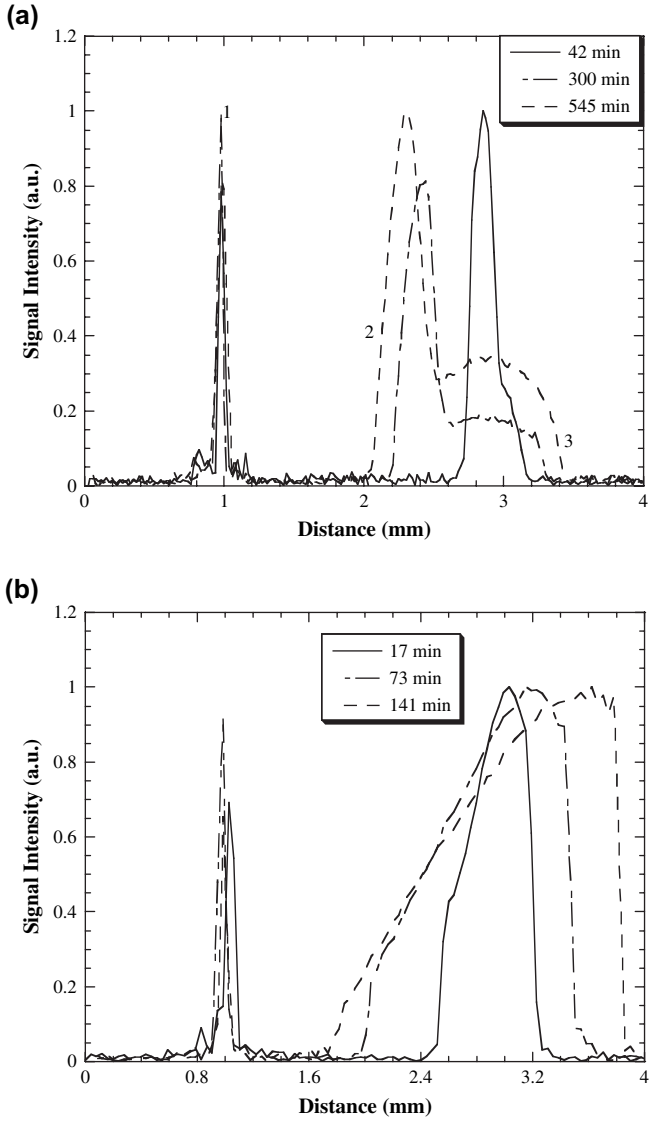

Fig. 8. MRI profiles obtained for the penetration of acetone into (a) polycarbonate and (b) PVC at 25 °C. In (a) label 1 refers to unexposed surface of the polymer disc, 2 refers to the leading edge of the acetone penetration front, and 3 refers to the exposed surface of the polymer disc.

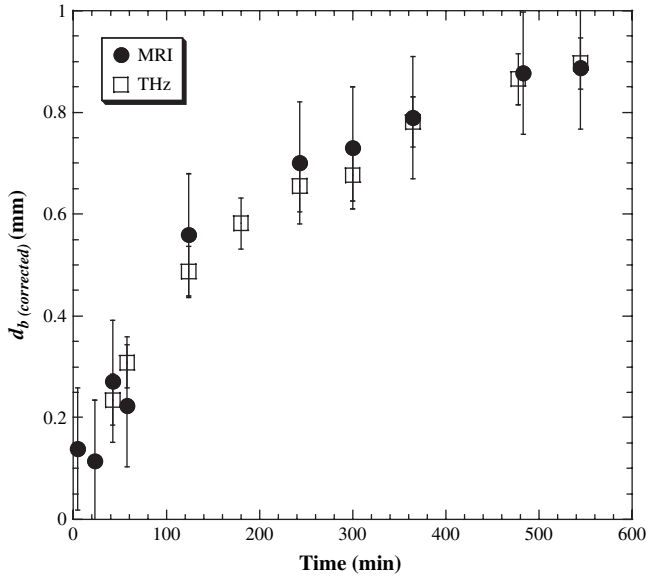

Fig. 9. Comparison of the penetration front of acetone into the polycarbonate discs at room temperature, corrected for swelling, as determined by MRI (●) and THz (□).

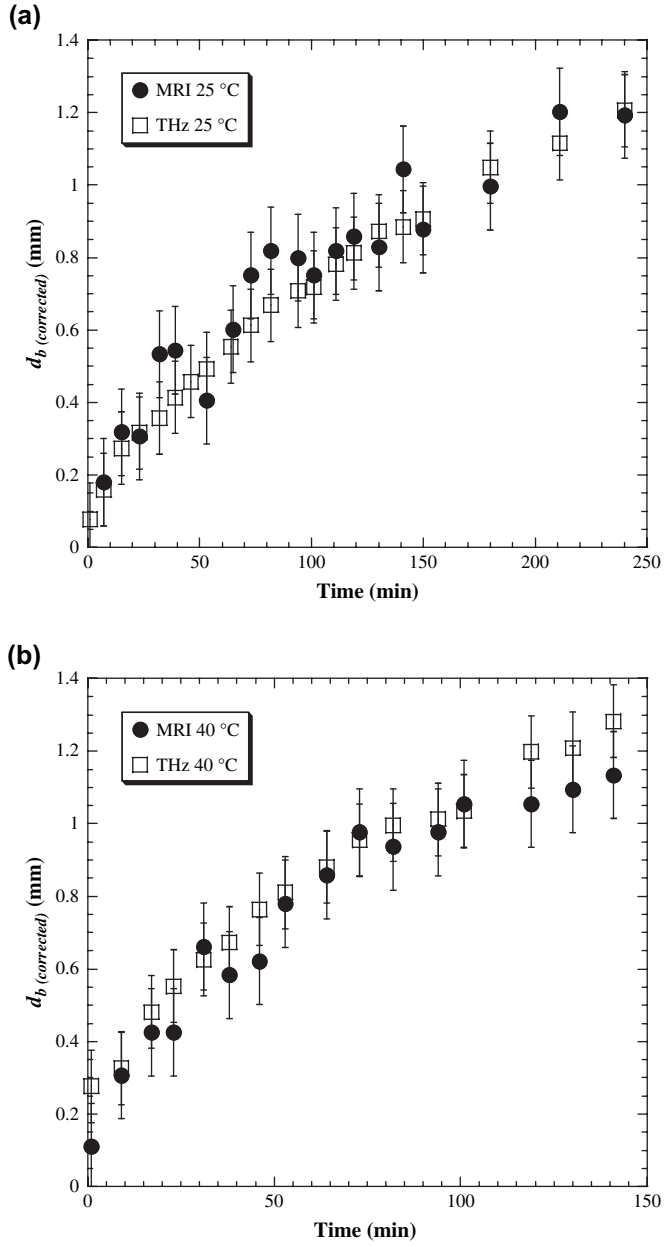

Fig. 10. Comparison of the penetration front of acetone into the PVC discs, corrected for swelling, as determined by MRI (●) and THz (□) at (a) 25 °C and (b) 40 °C.

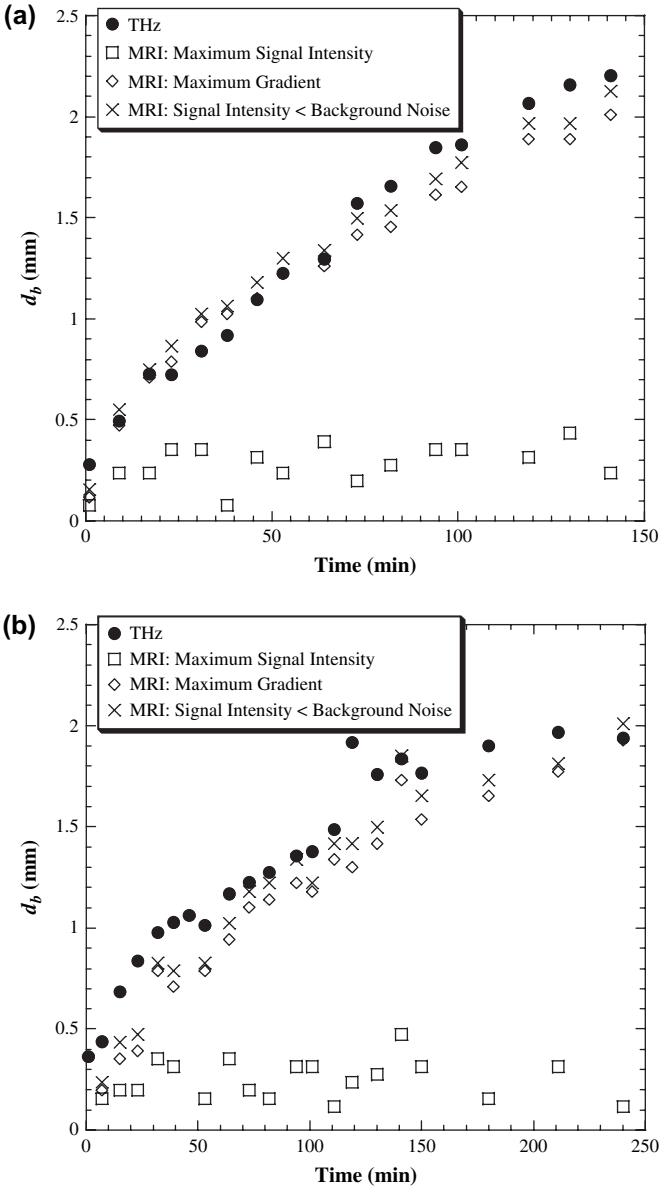

Fig. 11. Comparison of the uncorrected penetration front of acetone into the PVC discs at (a) 40 °C and (b) 25 °C. The THz (●) measurement is compared to possible acetone penetration fronts as determined from the MRI profiles. These are the point of maximum signal intensity (□), the point of maximum change in signal intensity (◇) and the point at which the signal intensity of the leading edge becomes less than the background noise (×).

close proximity, and that it is from this region of the front that the observed THz reflection originates.

4.3. Characterisation of front penetration

Application of Eq. (1) to the THz measurements of d_b in Fig. 5(b) for the polycarbonate data provided values for m and K of 0.45 and $6.7 \times 10^{-6}\,\mathrm{ms}^{-m}$, respectively ($R^2 = 0.994$). Thus the front was found to increase in length approximately with the square root of time, suggesting Case 1 behaviour. This is in agreement with the results presented by Turska and Benecki [29]. Crystallisation of the polycarbonate occurs behind the acetone penetrant [29,30]. The polycarbonate is initially in an amorphous state, with a crystallisation temperature much higher than room temperature. The acetone allows the polymer chains to have an increased mobility, significantly lowering the energy required for crystallisation to occur. Due to a time induction delay in the crystallisation, there occurs a certain distance behind the penetration front. This we believe causes the leading peak in the acetone concentration, evident in the MRI data in Fig. 8(a), followed by a dip in acetone concentration and signal where crystallisation is occurring, due to both concentration and local enhanced signal relaxation effects. Application of Eq. (1) to the PVC data presented in Fig. 7(a) results in the values of m and K (and the corresponding quality of the fit – R^2)

Table 1
Values of m for PVC

Temperature (°C)	d_b (THz)		
	m	K (ms^{-m})	R^2
13	0.49	8.7×10^{-7}	0.996
25	0.48	7.7×10^{-6}	0.965
40	0.45	1.5×10^{-5}	0.988

presented in Table 1. The values of m are consistently approximately 0.5, thus we can conclude that acetone ingress into PVC can be classified as a Case 1 process over the temperature range considered. This is in agreement with literature observations [4] based on mass uptake.

5. Conclusion

A novel measurement method of determining liquid ingress into polymer systems was presented using terahertz (THz) time-domain reflectance spectroscopy. The method was successfully applied to the ingress of acetone into both polycarbonate and PVC. Good agreement with respect to the penetrant front position was produced for both materials when compared with corresponding MRI data. In the case of the PVC, a broad penetrant front was evident, yet a distinct reflection was still produced by the leading edge. The use of THz time-domain reflectance spectroscopy in this capacity offers several advantages: it is not geometrically constrained and hence readily applied to any polymer geometry and it offers comparatively deeper beam penetration into samples. At present the depth resolution is relatively course and it only determines the location of a diffusion front. Future work will thus focus on improving the depth resolution and on analysis of the frequency spectrum from this pulse reflected by the wet polymer–dry polymer interface to see if it can provide information on the polymer conformation. Our work thus suggests that THz techniques can provide a useful tool for characterizing liquid mobility, and potentially conformational changes, that occur during liquid ingress into polymeric systems.

Acknowledgements

Financial support from a RC Basic Technology grant (GR/R87086/02) is gratefully acknowledged. JHPC also thanks MS&D for financial support.

Appendix A

Path length difference in polymer x_2 (Fig. 4):

$$\cos\beta = \frac{d_a}{x_2/2} \Rightarrow x_2 = \frac{2d_a}{\cos\beta}. \quad \text{(i)}$$

Shift of the reflection point a (Fig. 4):

$$\sin\beta = \frac{a/2}{x_2/2} \Rightarrow a = 2d_a\frac{\sin\beta}{\cos\beta} = 2d_a\tan\beta. \quad \text{(ii)}$$

Path length difference in air x_1 (Fig. 4):

$$\sin\alpha = \frac{x_1}{a} \Rightarrow x_1 = a\sin\alpha = 2d_a\tan\beta\sin\alpha. \quad \text{(iii)}$$

Overall path length difference Δx:

$$\Delta x = x_2 - x_1 = \frac{2d_a - 2d_a\sin\beta\sin\alpha}{\cos\beta} = \frac{2d_a}{\cos\beta}(1-\sin\beta\sin\alpha). \quad \text{(iv)}$$

Using Snell's law [25]:

$$\frac{\sin\alpha}{\sin\beta} = \frac{n_2}{n_1}, \quad \text{(v)}$$

Eq. (iv) becomes:

$$\Delta x = \frac{2d_a}{\cos\beta}\left(1 - \frac{n_1}{n_2}\sin^2\alpha\right). \quad \text{(vi)}$$

The time delay Δt at the detector introduced by the additional path length Δx is given by:

$$\Delta t = t_2 - t_1 = \frac{x_2 n_2}{c} - \frac{x_1 n_1}{c} = \frac{2d_a(t)}{c\cos\beta}(n_2 - n_1\sin\beta\sin\alpha). \quad \text{(vii)}$$

References

[1] Hyde TM. Transport in polymers: application to controlled drug release. PhD thesis, University of Cambridge, Cambridge, UK; 1995 [chapter 1].
[2] Harding SG, Johns ML, Pugh SR, Fryer PJ, Gladden LF. Food Addit Contam 1997;14:583–9.
[3] Ouyang H, Wu MT, Ouyang W. J Appl Phys 2004;96:7066–70.
[4] Simionescu CI, Topor C. Die Angew Makromol Chem 1998;257:31–5.
[5] Hung GWC. Microchem J 1974;19:130–52.
[6] Thomas NI, Windle AH. Polymer 1981;22:627–39.
[7] Fieldson GT, Barbari TA. Polymer 1993;34(6):1146–53.
[8] Clough AS, Collins SA, Gautlett FE, Hodgson MR, Jeynes C, Rihawy MS, et al. J Membr Sci 2006;285:137–43.
[9] Richman DJ, Long FA. J Am Chem Soc 1960;82:509–13.
[10] Hyde TM, Gladden LF. Polymer 1998;39:811–9.
[11] Dutheillet Y, Mantle M, Vesely D, Gladden L. J Polym Sci B Polym Phys 1999;37:3328–36.
[12] Ferguson B, Zhang XC. Nat Mater 2002;1:26–33.
[13] Kimmitt MF. J Biol Phys 2003;29:77–85.
[14] Chamberlain JM. Philos Trans R Soc London Ser A 2004;362:199–213.
[15] Mittleman DM, Jacobsen RH, Nuss MC. IEEE J Sel Top Quantum Electron 1996;2(3):679–91.
[16] Woodward RM, Wallace VP, Cole BE, Pye RJ, Arnone DD, Linfield EH, et al. Phys Med Biol 2002;47:3853–63.
[17] Crawley D, Longbottom C, Wallace VP, Cole B, Arnone D, Pepper M. J Biomed Opt 2003;8(2):303–7.
[18] Upadhya PC, Nguyen KL, Shen YC, Obradovic J, Linfield EH, Fukushinge K, et al. Spectrosc Lett 2006;39:215–24.
[19] Fitzgerald AJ, Cole BE, Taday PF. J Pharm Sci 2005;94:177–83.
[20] Pickwell E, Cole BE, Fitzgerald AJ, Pepper M, Wallace VP. Phys Med Biol 2004;49:1595–607.
[21] Alfrey T, Gurnee EF, Lloyd WG. J Polym Sci C 1966;12:249–61.
[22] Wang TT, Kwei TK, Frisch HL. J Polym Sci A-2 1969;7:2019–28.
[23] George SC, Thomas S. Prog Polym Sci 2001;26:985–1017.

[24] Cai Y, Brener I, Lopata J, Wynn J, Pfeiffer L, Federici J. Appl Phys Lett 1997;71:2076–8.
[25] Dykaar DR, Greene BI, Federici JF, Levi AFJ, Pfeiffer LN, Kopf RF. Appl Phys Lett 1991;59(3):262–4.
[26] Hecht E. Optics. 2nd ed. Addison-Wesley Publishing Company; 1974.
[27] Shen YC, Upadhya PC, Beere HE, Linfield EH, Davies AG, Gregory IS, et al. Appl Phys Lett 2004;85(2):164–6.
[28] Kumar A, Welti D, Ernst R. J Magn Reson 1974;18:69–83.
[29] Turska E, Benecki W. J Appl Polym Sci 1979;23:3489–500.
[30] Ercken M, Adriaensens P, Vanderzande D, Gelan J. Macromolecules 1995;28:8541–7.